



## **Impact of Accelerated Stress Tests on the Cathodic Catalytic Layer in a Proton Exchange Membrane (PEM) Fuel Cell Studied by Identical Location**

Downloaded from: <https://research.chalmers.se>, 2025-12-10 01:14 UTC

Citation for the original published paper (version of record):

Shokhen, V., Strandberg, L., Skoglundh, M. et al (2022). Impact of Accelerated Stress Tests on the Cathodic Catalytic Layer in a Proton Exchange Membrane (PEM) Fuel Cell Studied by Identical Location Scanning Electron Microscopy. ACS Applied Energy Materials, 5(9): 11200-11212. <http://dx.doi.org/10.1021/acsaem.2c01790>

N.B. When citing this work, cite the original published paper.

# Impact of Accelerated Stress Tests on the Cathodic Catalytic Layer in a Proton Exchange Membrane (PEM) Fuel Cell Studied by Identical Location Scanning Electron Microscopy

Victor Shokhen,<sup>\*,†</sup> Linnéa Strandberg,<sup>†</sup> Magnus Skoglundh, and Björn Wickman<sup>\*</sup>



Cite This: *ACS Appl. Energy Mater.* 2022, 5, 11200–11212



Read Online

ACCESS |



Metrics & More



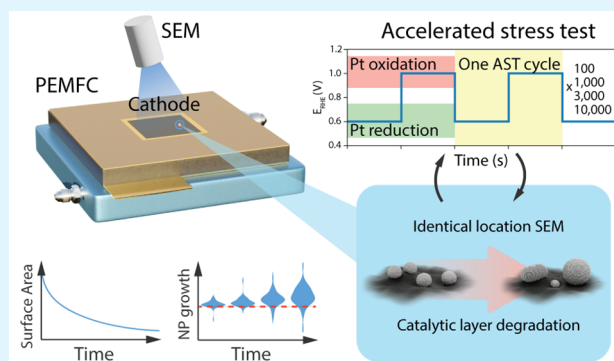
Article Recommendations



Supporting Information

**ABSTRACT:** Platinum is the most used electrocatalyst in proton exchange membrane fuel cells (PEMFCs). Nonetheless, it suffers from various types of degradation. Identical location electron microscopy has previously been used to observe local catalyst changes under accelerated stress tests (ASTs), giving insight into how individual catalyst particles degrade. However, it is important that such studies are carried out under relevant reaction conditions, as these can differ substantially between liquid half-cells and real PEMFC conditions. In this work, a single cell PEMFC was used to study the degradation of a commercial Pt-catalyzed membrane electrode assembly by performing square wave voltage ASTs in a potential range of 0.6 to 1.0 V. Identical location scanning electron microscopy (IL-SEM) was used to follow the degradation of the cathodic catalytic layer (CL) throughout 14,000 AST cycles. From the IL-SEM, we can conclude that the Pt nanoparticles degrade via Ostwald ripening, crystal migration, and coalescence. Small Pt nanoparticles agglomerate to larger particles or dissolve and redeposit to more stable particles, increasing the average particle size during the ASTs. In addition, cross-sectional TEM images show thinning of the ionomer layer during the AST procedure. The IL-SEM technique facilitates observation of local degradation of the CL in real PEMFCs, which will help to understand different degradation mechanisms, allowing for better solutions to be designed.

**KEYWORDS:** PEMFC, platinum, catalytic layer degradation, catalyst deactivation, accelerated stress test, identical location-SEM



## INTRODUCTION

Our society needs to move away from fossil-fuel-based energy sources to renewable sources of energy, such as solar and wind power, and switch to sustainable carbon-emission free alternatives for energy storage and fuels such as hydrogen-based alternatives.<sup>1,2</sup> Two promising technologies in these areas are fuel cells and electrolyzers, both of which are under intense research to make them more efficient for commercial use. Hydrogen can be generated by electricity from renewable energy sources by electrolyzers and can later be stored and converted back to electricity in fuel cells.<sup>3,4</sup> Proton exchange membrane fuel cells (PEMFCs), which are based on acidic membranes, produce electricity by oxidizing H<sub>2</sub> by O<sub>2</sub> to produce electricity and pure water, without CO<sub>2</sub> emissions. PEMFCs are suitable for long-range transportation, such as heavy-duty transport, passenger cars, and marine vehicles, and increasing the use of nonfossil hydrogen as fuel in these applications will help reduce the overall CO<sub>2</sub> emissions from the transport sector.<sup>5–7</sup>

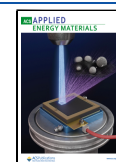
PEMFCs are already in use in several commercial applications, but they still have stability issues and performance barriers that need to be overcome.<sup>6,8</sup> To make PEMFCs

perform well, they require a catalyst to facilitate the oxidation of H<sub>2</sub> by O<sub>2</sub>. Catalysts in PEMFCs have to endure varying operational conditions such as fuel and air starvation,<sup>9</sup> start-up and shut-down events,<sup>10,11</sup> and varying loads,<sup>12,13</sup> temperatures,<sup>14</sup> and relative humidity (RH).<sup>15,16</sup> In commercial PEMFCs, Pt nanoparticles supported on carbon are used as the catalyst in both the anode and the cathode catalyst layer (CL) of the membrane electrode assembly (MEA) due to the high activity and stability of Pt in these harsh conditions compared to its alternatives.<sup>17</sup> However, Pt is both expensive, which contributes to a high production cost of PEMFCs, and suffers from several challenges related to degradation.<sup>18,19</sup> Although Pt is a stable element, the high and varying potentials during fuel cell operation can promote corrosion of Pt and its

Received: June 8, 2022

Accepted: August 8, 2022

Published: August 18, 2022



dissolution, especially on the cathodic side.<sup>20,21</sup> Repeated shifts between oxidizing and reducing potentials cause Pt to cycle between metallic and oxidized states, which can result in dissolution and changes of the surface structure over time.<sup>18,19,22</sup> Most of the dissolved Pt ions will later redeposit on other nanoparticles. On average, the Pt ions tend to deposit on larger particles which are more stable, causing smaller particles to shrink and larger neighbor particles to grow in a process known as Oswald ripening.<sup>23–25</sup> Furthermore, Pt ionic species can be redistributed across the MEA via the channels of the ionomer, which is a polymer electrolyte that conducts protons from the anode to the cathode,<sup>26,27</sup> and redeposit at new locations, such as inside the polymer electrolyte membrane, and form new Pt particles, which usually occurs in the case of H<sub>2</sub> crossover.<sup>28,29</sup>

Apart from the catalyst, PEMFCs also suffer from degradation of the polymer electrolyte and the carbon support. The ionomer of the PEMFC must have high proton conductivity and good contact with the catalyst to allow maximum performance.<sup>30–32</sup> Degradation of the ionomer will reduce the performance of the cell.<sup>33,34</sup> Ionomer degradation can be induced by several factors, such as mechanical degradation in the form of uneven pressure in the MEA due to the shrinking and swelling of the membrane caused by varying RH levels.<sup>13</sup> Dissolved catalyst material or other contaminating ions can bind to the sulfonic acid sites of the ionomer and thus block the proton conductivity. Moreover, chemical degradation of the ionomer can occur when it reacts with free radicals in the system.<sup>33,35</sup> The carbon support can suffer from degradation during fuel cell operation in the carbon oxidation reaction (COR).<sup>36,37</sup> The COR begins at a potential of about 0.2 V vs the reversible hydrogen electrode (RHE). However, due to the slow kinetics of the COR, the rate of degradation is negligible below 1.0 V<sub>RHE</sub>.<sup>38</sup> Even so, carbon corrosion can occur at start-up/shut-down events or during fuel and air starvation.<sup>9,39</sup> These events cause the potential to peak outside the normal operation range, which can result in COR of the carbon support and deformation of the CL. Over time, this leads to thinning of the CL, which is often called “cathodic thinning”.<sup>40,41</sup> The COR can also promote migration of Pt nanoparticles around the support, which can lead to agglomeration of nanoparticles, and strong COR can even cause the catalyst nanoparticles to detach from the support.<sup>38,42,43</sup>

The degradation of the catalyst, ionomer, and carbon support leads to irreversible damage of the CL over time, reducing the available electrochemical surface area (ECSA) of the nanoparticles, as well as the overall performance of the fuel cell.<sup>12,29,44,45</sup> Degradation studies are essential to understand the behavior of the CL and what causes it to degrade, so that PEMFCs with increased life spans can be designed.<sup>28,33,44,46</sup> Studies of fuel cell degradation are often focused on the active and sensitive part of the MEA, such as the CL and the membrane. In particular, much attention has been given to the cathodic CL due to the oxygen reduction reaction (ORR), which, due to its multistep reaction pathway,<sup>47</sup> is slower than the hydrogen oxidation reaction (HOR), hence a higher loading of Pt is required on the cathodic CL compared to the anodic CL.<sup>48,49</sup>

There are several techniques to study fuel cell degradation, for example by analyzing the electrochemical performance complemented with ex situ and in situ measurements and characterization.<sup>19,28,29,33,50</sup> One approach that has been used

to observe catalyst aging is microscopy imaging from the beginning and end of life, often from different areas of the CL.<sup>11,18</sup> To gain more quantitative data of the degradation, identical-location (IL) techniques can be used to study the behavior and degradation of individual Pt nanoparticles.<sup>51</sup> IL transmission electron microscopy (IL-TEM) has previously been used to study the degradation of electrocatalysts such as Pt/C, Pd/C, and alloys by casting the electrocatalysts on TEM grids and performing electrochemical accelerated stress test (AST) procedures on the grids in liquid half-cell setups.<sup>12,52,53</sup> IL-TEM has also been utilized to study the degradation of Pt and PtCo catalysts and how it is affected by varying parameters such as Pt-ion concentration, temperature, acid conditions, ionomer content, and voltage ranges.<sup>54</sup> Another IL technique that has also been utilized to study catalyst degradation is IL scanning electron microscopy (IL-SEM), which has been used to study the degradation of Pt/C catalysts on a rotating disk electrode (RDE) in liquid half-cell setups.<sup>55,56</sup> Moreover, a comparison between the IL-TEM and IL-SEM techniques has been made with the Pt alloy catalysts PtNi and PtCu.<sup>57</sup>

Although those studies show quantitative observations of local degradation of catalysts, the ASTs in liquid electrolyte environments are different from those in a real PEMFC based on solid membrane electrolytes in a polymer form.<sup>58</sup> Degradation does not necessarily transpire in the same fashion in liquid cells as in gas cell conditions,<sup>59</sup> making the results difficult to translate to real PEMFC applications. To observe the degradation of Pt/C via IL-TEM under more realistic PEMFC conditions, studies have been made using a gas diffusion electrode setup.<sup>60</sup>

Even so, it is of interest to use IL methods to study degradation during actual fuel cell operational conditions. However, there are several challenges with in-depth fuel cell degradation studies due to the size and shape of the closed PEMFC system, making it hard to insert tools for analysis without damaging the MEA or the supporting structures. To circumvent this problem, some studies are performed using unique custom-made fuel cell designs that allow for in situ observation of the degradation.<sup>61,62</sup> IL-SEM imaging can help with gaining better understanding of the CL degradation processes in real PEMFC systems.<sup>63</sup> In particular, it is of interest to study the degradation of the CL in traditional fuel cell operation conditions of below 1.0 V<sub>RHE</sub>, to avoid degradation caused by carbon corrosion while still obtaining fundamental observations of the aging of the Pt nanoparticles.<sup>12,44,50</sup> This type of technique can help with understanding the real nature of CL degradation and help provide more suitable solutions for, e.g., CL design and drive cycles.

In this study, IL-SEM is used to observe the degradation of the cathodic CL under normal PEMFC operational conditions between 0.6 and 1.0 V<sub>RHE</sub> at 80 °C and with fully humidified gases. With the IL-SEM technique, the aging of individual regions and particles of a commercial MEA in a full single-cell PEMFC can be tracked during a square wave (SW) accelerated stress test. From the IL-SEM imaging we can conclude that the Pt nanoparticles in the cathodic CL age mainly by a combination of Oswald ripening, and crystallite migration and coalescence. The average Pt particle size increase during the aging process was about 35%, although some particles shrink. In addition, cross-sectional TEM images show thinning of the ionomer layer during the AST procedure. The increased particle size and thinning of the ionomer layer result in a

decrease of the electrochemical active surface area by about 72% at the end of the AST.

## EXPERIMENTAL PART

**Fuel Cell Testing System. Membrane Electrode Assembly.** In all experiments, commercial three-layer catalyst coated membranes (CCMs) with an active area of  $5\text{ cm}^2$  were used (Ion Power Inc), with a catalytic layer loading of  $0.1/0.4\text{ mg}_{\text{Pt}}\text{ cm}^{-2}$  on the anode/cathode, respectively. The CCMs were sandwiched between two gas diffusion layers (GDLs) (SGL SIGRACET GDL 36 BB) to form the MEA. The GDL compression of approximately 20% was adjusted by fiberglass gaskets reinforced with PTFE (Fiberflon GmbH).

**Fuel Cell Setup.** The electrochemical procedures were conducted in a single-cell fuel cell with an active area of  $5\text{ cm}^2$  (Scribner Associates Inc), with serpentine graphite flow fields. The cell was assembled with a torque force of 12 N m. The test bench is an in-house-built test station, and the gas was fed through heated humidity bottles and gas tubes before entering the fuel cell. The flow of the gases was controlled by mass flow controllers (Bronkhost High-Tech BV). The gas in the system was under atmospheric pressure. The electrochemical measurements were controlled and analyzed by a potentiostat (HCP-803 Bio-Logic) equipped with an 80 A amplifier. All potentials were measured, and are presented, against the reversible hydrogen electrode.

**Electrochemical Protocols. Activation Procedure.** Prior to electrochemical testing, all MEAs were put through a conditioning procedure using  $\text{H}_2/\text{air}$  with a gas flow of 140/400 nccm on the anode/cathode at  $60\text{ }^\circ\text{C}$  and a relative humidity (RH) of 100%. The activation procedure consisted of chronoamperometry (CA) cycles where the voltage was held at 0.6 V for 45 min, 0.95 V for 5 min, and then 0.85 V for 10 min. This sequence was repeated 10 times.

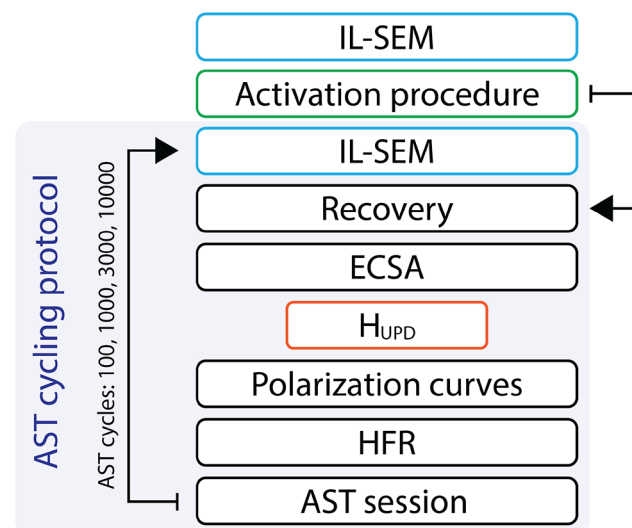
**Recovery Step.** A recovery step was performed after the activation procedure and before each new AST session to recover reversible losses. The process was done with  $\text{H}_2/\text{air}$  with a flow of 140/400 nccm (anode/cathode), at a cell temperature of  $40\text{ }^\circ\text{C}$ . The recovery was done by holding the voltage at 0.3 V for 2 h at 100% RH.

**Cyclic Voltammograms (CVs).** CVs were performed by sweeping the cathode electrode potential between 0.07 and  $1\text{ V}_{\text{RHE}}$  at scan rates of 150, 100, and  $50\text{ mVs}^{-1}$  at  $40\text{ }^\circ\text{C}$  and with gas flows of 20/5 nccm  $\text{H}_2/\text{Ar}$  (anode/cathode). The CV sweep performed at  $100\text{ mV s}^{-1}$  was used to calculate the electrochemically active surface area (ECSA) from the underpotential deposition of hydrogen  $\text{H}_{\text{upd}}$  values using a surface charge of  $210\text{ }\mu\text{C cm}^{-2}$  of Pt for polycrystalline Pt<sup>64</sup> and assuming a 100% coverage.

**Accelerated Stress Test (AST).** The measurements were done by using square-wave ASTs consisting of potential cycling between 0.6  $\text{V}_{\text{RHE}}$  and  $1.0\text{ V}_{\text{RHE}}$  at 16 s per cycle (8 s hold at each potential point).<sup>44</sup> The AST was done with  $\text{H}_2/\text{Ar}$  with flows of 100/75 nccm (anode/cathode),<sup>63</sup> at a cell temperature of  $80\text{ }^\circ\text{C}$  and with 100% RH. The system was cycled for an overall total of 14,100 cycles, in AST sessions consisting of 100, 1000, 3000, and 10,000 cycles each. See Figure 1 for an overview of the testing procedure.

**Physical Characterization. Identical-Location Scanning Electron Microscopy (IL-SEM).** Prior to the activation procedure, and after each AST session, the cathode layer was imaged using IL-SEM. First, the MEA was assembled fully according to Figure 2a and inserted into the fuel cell to press it together (Figure 2b). After the initial assembly, and after each AST session, the MEA was removed from the fuel cell, and the GDL of the cathodic side was gently removed leaving no trace or signs of the GDL adhering to the catalyst layer, exposing the cathodic catalyst layer (Figure 2c). As a side note, while the GDL on the cathode side was possible to remove without signs of damage to the cathodic catalyst layer, the GDL on the anode side consistently became merged with the anode catalyst layer, as noted when tested on other samples. The MEA, with the cathodic GDL removed, was inserted into the SEM (Zeiss Ultra 55 FEG) on an in-house-built holder ensuring the same position every time, and together with tracking coordinates, this enabled identification of the same location repeatedly without any physical marking of the catalyst layer being

a



b

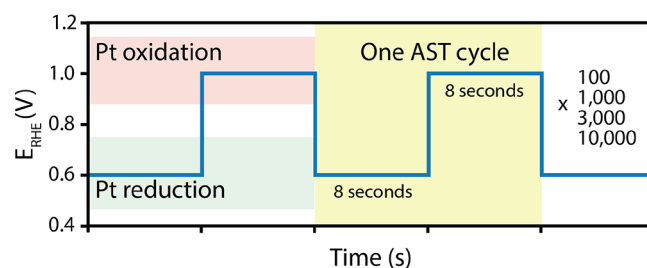


**Figure 1.** (a) Overview of the experimental methodology for MEA aging with and without IL-SEM after each AST session. (b) Square wave voltage profile that was used for the AST cycling. The square wave consisted of potential holds at 0.6  $\text{V}_{\text{RHE}}$  and 1.0  $\text{V}_{\text{RHE}}$ , the reduction and oxidation potential points of platinum, respectively. Each potential hold time is 8 s with an overall of 16 s per AST cycle, which were repeated 100, 1000, 3000, and 10,000 times per AST session, respectively, for an overall total of 14,100 AST cycles.

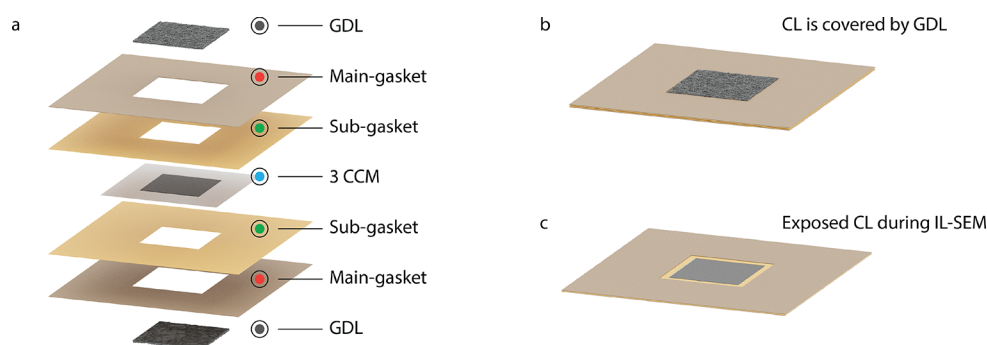
necessary. The cathodic catalyst layer was imaged using an accelerating voltage of 5 kV with the same working distance each time. After imaging, the GDL was placed back on top of the CL, and the full MEA was reinserted into the fuel cell. To ensure that the repeated disassembling/reassembling of the fuel cell and SEM imaging of the catalyst layer did not affect its performance, a second experiment was run for reference following the same electrochemical protocol but without any interruption of the fuel cell such as disassembling or imaging of the fuel cell in between AST sessions.

**Transmission Electron Microscopy.** Thin lamellas were prepared from one fresh sample and one sample at end of life (EOL) using focused ion beam (FIB) (FEI, Versa3D). TEM images of the lamellas were obtained by high-resolution TEM (HRTEM) using an FEI Tecnai G2 F20 instrument operating at 200 kV.

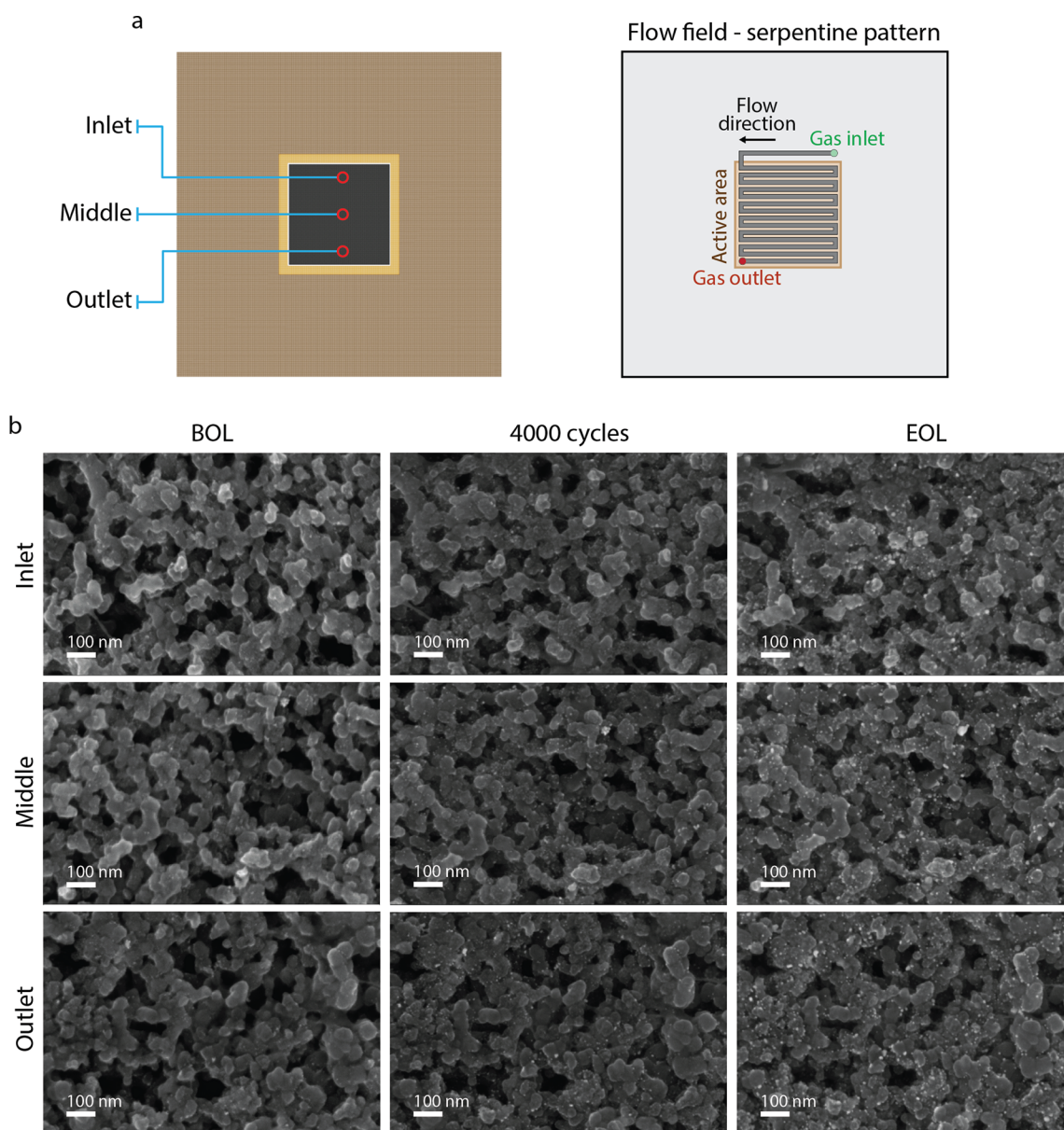
## RESULTS AND DISCUSSION

Figure 1a presents the methodology of the experiment, which started with IL-SEM to observe the fresh state of the surface of the catalytic layer, followed by a conditioning procedure to activate the MEA, and, after that, continued to the AST cycling protocol. The fuel cell experiment was carried out in a fully humidified cell at ambient pressure, and the cycling protocol started with a recovery procedure to recover reversible losses. To evaluate how the AST affected the cell performance, several





**Figure 2.** Schematic illustrations of (a) all layers in the membrane assembly and their order in relation to each other, (b) a fully assembled MEA, and (c) an MEA with the top GDL removed to expose the cathode catalytic layer during IL-SEM.



**Figure 3.** (a) Position of the inlet, middle, and outlet regions on the MEA from where the IL-SEM images were taken. The right image illustrates the gas flow from the flow field in a serpentine pattern. (b) Images from respective positions at beginning of life, after 4000 completed cycles and at the end of life.

electrochemical experiments were done. After the recovery procedure, the electrochemically active surface area was

measured by performing cyclic voltammetry in a potential range of 0.07 to 1.0  $V_{RHE}$  at three different scan speeds using

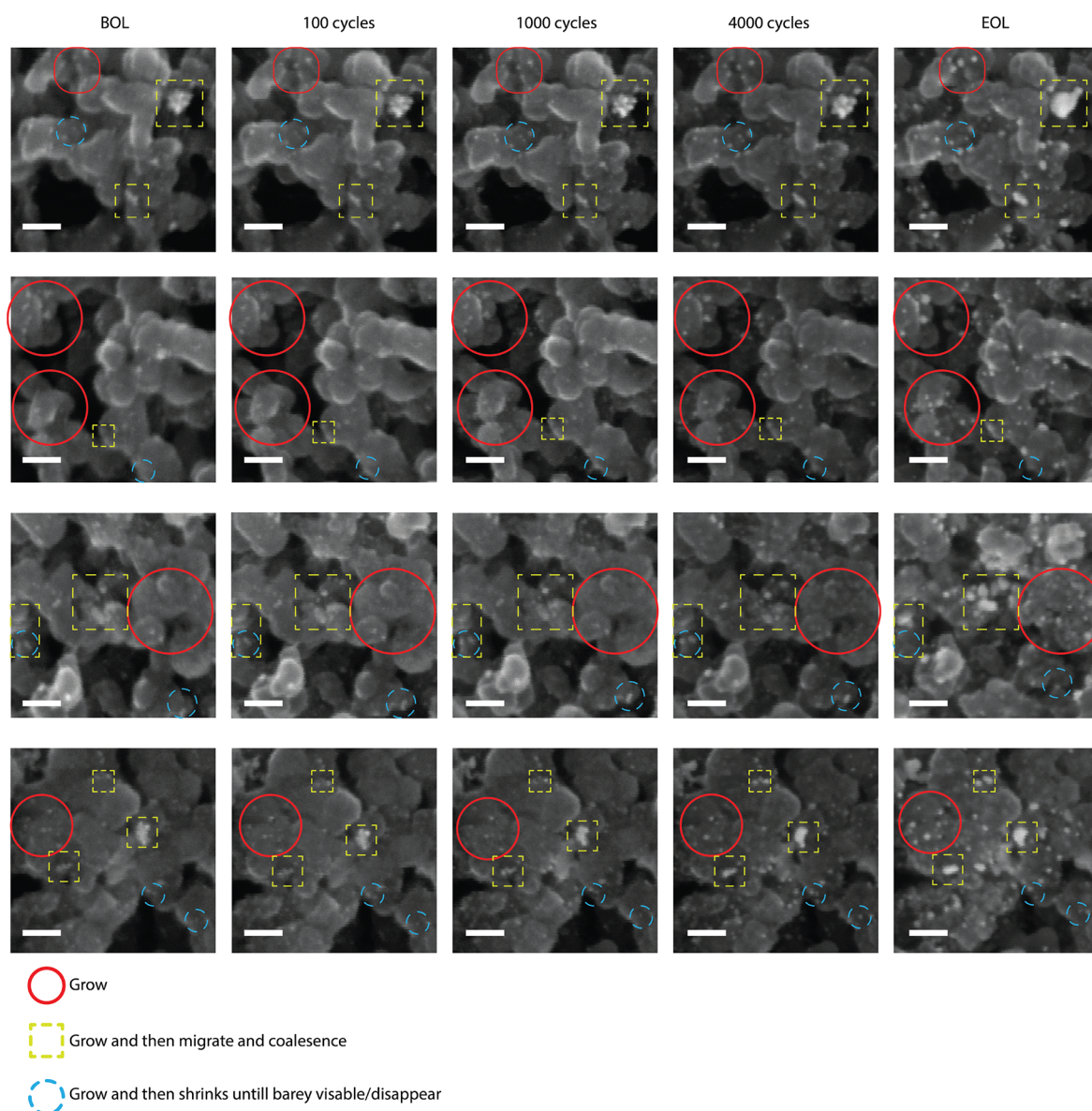


**Figure 4.** Representative IL-SEM images of the cathodic catalytic layer highlighting different types of catalyst changes from BOL (fresh) to after each AST session until EOL (14,000 cycles overall). The red circles mark general growth of particles, the yellow dashed square shows particles that migrate and coalesce, and the blue dashed circle represents particles that first grow and then shrink. The markers are not comprehensive and only illustrate the main degradation effects during the AST cycling procedure. Scale bar = 50 nm.

H<sub>2</sub>/Ar (anode/cathode), and integrating the charge associated with hydrogen underpotential deposition (H<sub>upd</sub>). The oxygen reduction reaction activity of the fuel cell was evaluated each protocol cycle together with the ohmic resistance of the cell, by measuring polarization curves together with high-frequency resistance (HFR) measurements. After electrochemical characterization, AST sessions were performed with an increased number of cycles for each protocol cycle. Figure 1b presents the AST used, which consisted of square wave (SW) potential scans between 0.6 and 1.0 V<sub>RHE</sub> with a hold time of 8 s at each potential and a period time of 16 s. The AST cycling protocols consisted of 100, 1000, 3000, and 10,000 SW cycles with an overall total of 14,100 cycles, which here is considered as the end of life (EOL). The AST sessions were performed with H<sub>2</sub>/Ar (anode/cathode) at 80 °C, 100% RH, and atmospheric pressure.

Initial IL-SEM images were taken before the activation procedure at the beginning of life (BOL), and then IL-SEM imaging was done after each AST session. Before the initial IL-SEM imaging, gas diffusion layers, main gaskets and subgaskets, and a commercial three-layer CCM were stacked and pressed together to form the MEA (Figure 2a and b). For IL-SEM imaging, the MEA was removed from the fuel cell, and the cathodic gas diffusion layer (GDL) was removed to expose the cathodic CL (Figure 2c). See the Experimental Part for details on the procedure. A separate experimental sequence was made following the same test protocol but with IL-SEM being performed only at the BOL and EOL, to evaluate if disassembling/assembling the fuel cell in between aging sessions affects its performance.

IL-SEM images were taken at three locations on the cathodic CL: near the gas inlet, in the middle, and near the outlet of the serpentine pattern flow field used for the gas



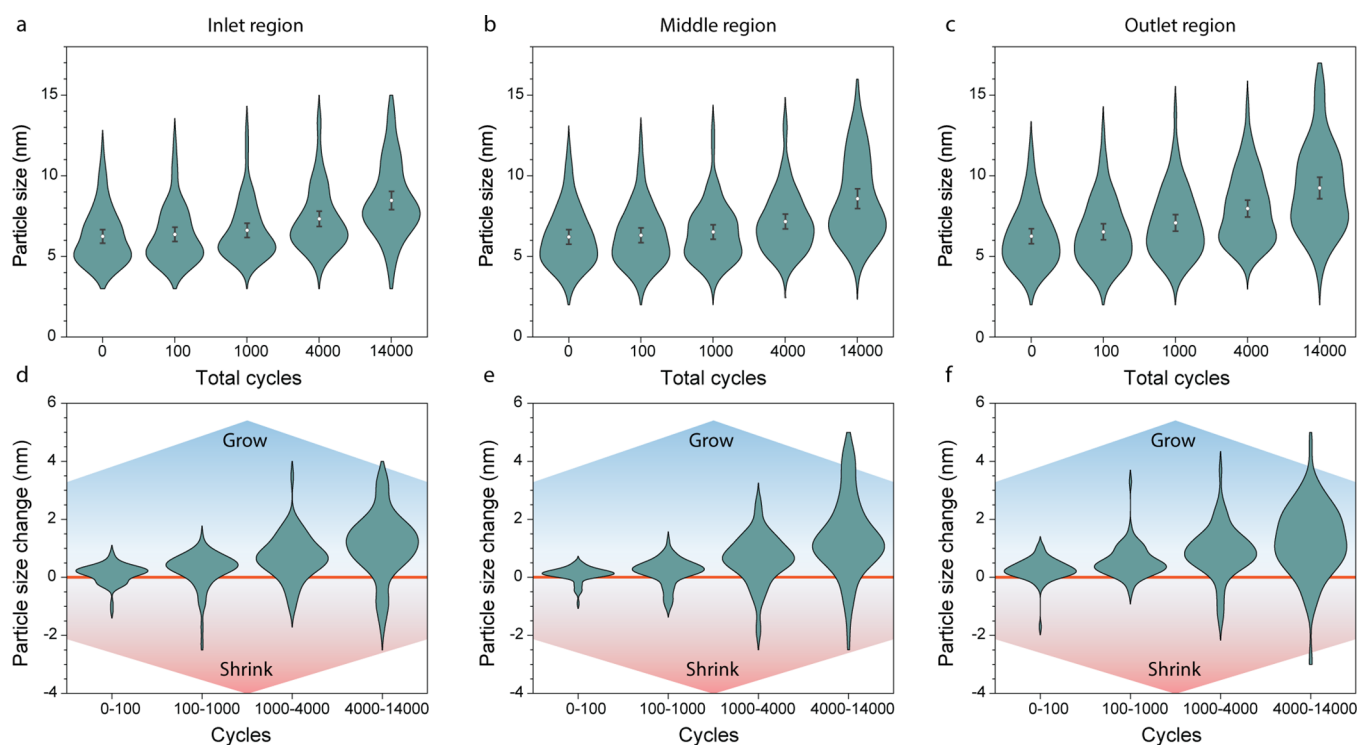


**Figure 5.** Particle size distribution at BOL and after 100, 1000, 4000, and 14,000 total cycles for (a) the inlet region, (b) the middle region, and (c) the outlet region. For each location, 65 particles were chosen from the initial image and tracked throughout the aging process, and their diameter were measured after each AST run. The white circles represent the mean size, and the standard error bars are shown as black lines. The size change of each individual particle during each AST run, defined as the change in diameter of that particle from the prior image, was calculated for (d) the inlet, (e) the middle, and (f) the outlet regions. Negative values represent particles that shrunk in size during the AST session.

channel flow (Figure 3a). For each location, images were taken at the BOL, after 100, 1000, and 4000 completed cycles, and at the EOL (14,100 cycles). Figure 3b presents images from the BOL, after 4000 cycles, and at the EOL, since those steps demonstrate more drastic differences. For images after 100 and 1000 cycles see the Supporting Information (SI) for full extended IL-SEM images. At the BOL, the SEM images show a porous CL made of carbon support with Pt nanoparticles dispersed on the surface of the support. After 4000 cycles, many particles have grown, and new particles have emerged seemingly from previously empty spots, which could be explained by these particles being too small to be observed by SEM at the BOL (Figure S1). At the EOL, most particles have grown even more, and many have moved and merged with neighbor particles to form larger particles. Further inspection also revealed that some particles have shrunk or even disappeared completely. Moreover, the carbon support has slightly deformed, and some carbon parts moved and got closer to neighbor carbon particles during the AST session, which slightly changed the porous structure of the CL. In a few regions, parts of the carbon support have completely detached and been lost.

Figure 4 shows a selection of high-magnification IL-SEM regions to further illuminate some of the main observed degradation effects. A majority of the particles that were observed by SEM have grown. However, it is important to note that some visible smaller particles have shrunk. To study the general growing pattern, 65 Pt particles from each location (inlet, middle, and outlet), visible by SEM at the BOL and in all subsequent images, were chosen to analyze the particle size distribution (PSD), and the size changes of those particles

were then tracked throughout the aging process. All particles remained visible in all images. Particles below the SEM detection level, about 3 nm, at the BOL are excluded from the PSDs, which skews the results and most likely overestimates the average particle size. Furthermore, due to the limited resolution and the subsequent difficulty in defining the exact edges of the particles, the error in measurement is estimated to be around 1 nm, which in larger particles above 10 nm gives a relative error of around  $\pm 10\%$ , while the smallest measured particles of around 3 nm have a relative error of up to  $\pm 30\%$ . However, the PSDs should still give insight on particle growth over time. To compare the growth patterns in the different regions, particles were selected at each location such that they formed similar PSD starting points (Figure 5a–c).

The selective initial PSDs are similar to each other, whereas their growth patterns differ between each region during the AST process. The particles grow more in size the further downstream they are located in the flow stream, as seen when comparing between the inlet and outlet regions. At the EOL, the PSD of the inlet is more concentrated around 7–8 nm, whereas at the regions further away from the inlet, the PSD is more spread out toward higher particle sizes. The disparity may be caused by the RH and gas flow not being constant over the flow field, resulting in variations in the dissolution and redeposition of Pt.<sup>65,66</sup>

Further insight can be retrieved by tracking the size change of each individual particle during each AST session (Figure 5d–f), defined as the change in size of each particle from the previous measurement. Most particles tend to grow during the AST sessions, reflecting the growth in average particle size, but some particles do shrink due to dissolution. The behavior of

the particles is similar in all three regions, with the particle growth being concentrated between 0 and 0.2 nm after 100 cycles. The particles, growth rate per AST cycle is higher up to 4000 cycles, after which the growth rate slows down, possibly indicating that the particles reach a more stable state and are less prone to changing.

From the PSD, the average particle size of the 65 chosen particles was calculated for each location and after each aging cycle (Figure 6). The average particle size increased from

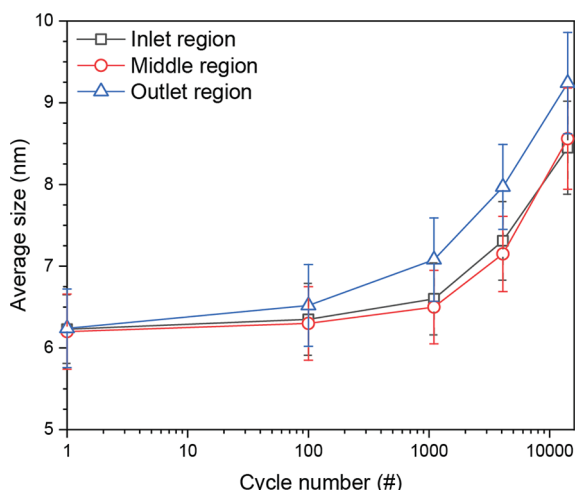


**Figure 6.** Average particle size with standard error bars at BOL and after a total of 100, 1000, 4000, and 14,000 cycles for the inlet region (black squares), the middle region (red circles), and the outlet region (blue triangles). For each location, 65 particles were chosen from the BOL image and tracked through the aging process, and the average diameter of those particles was measured after each AST run.

about 6.2 nm at the BOL for all regions to around 8.5 nm for inlet and middle points and 9.2 nm at the outlet at the EOL. The measured average particle size is high compared to the average size of commercial nanoparticles, which is around 2–3 nm in diameter (Figure S1b), but the results are skewed due to particles in that size range not being visible by SEM. Still, there are some nanoparticles that are larger than 2–3 nm at the BOL which are visible by SEM.

To gain more information on the smaller particles and the behavior throughout the catalyst layer, representative TEM images were taken of lamella slices that were extracted with FIB from the cathodic side of two CCMs: one from the BOL (Figure 7a and b) and another at the EOL (Figure 7c and d). The fresh MEA is homogeneously covered with Pt nanoparticles with an average size of about 2 nm, together with some larger particles (>5 nm) and particle clusters. Figure S2 shows additional TEM images of the cathodic CL sample at the BOL. Most of these particles are too small to be visible in SEM, which explains why the SEM images of the BOL seem to be almost clear from Pt particles, with some larger particles dispersed throughout. While a PSD calculated from the TEM images would give a more accurate representation of the PSD at the BOL than the PSD calculated from the SEM images, it could not be used to measure the growth of individual particles, which is one of the strengths of using IL-SEM imaging. TEM images of the cathodic CL at the EOL reveal a significant change of the Pt particles. The carbon support is no longer homogeneously covered with Pt nanoparticles but shows large empty areas, and the Pt particles that remain are

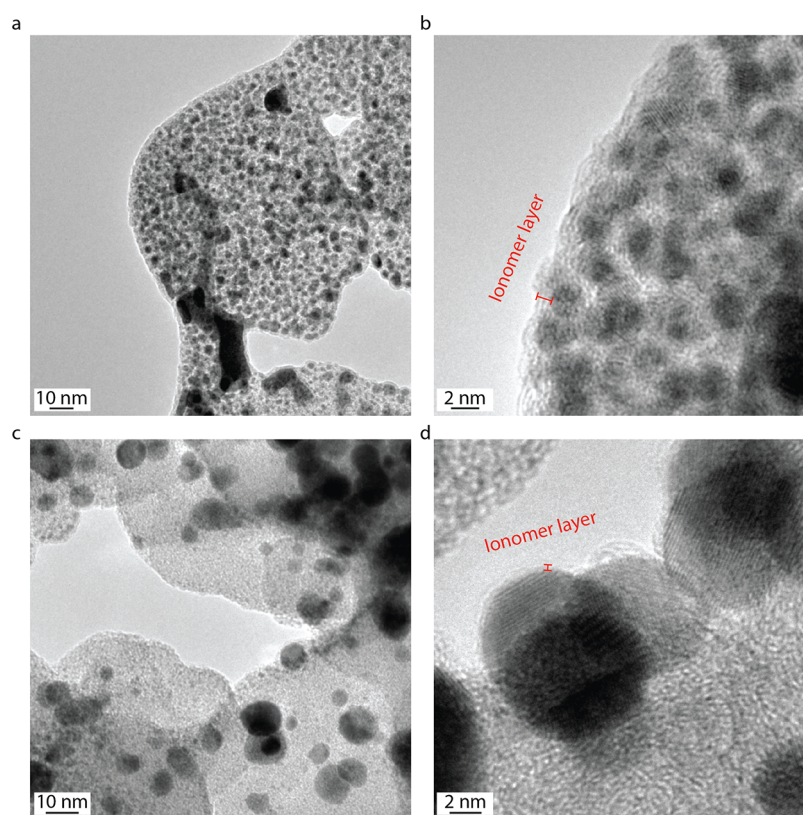
much larger in size than at the BOL. This indicates that the smaller particles have migrated and merged, forming fewer but larger particles. At the BOL, the catalytic layer is coated with an organic overlayer that, since it is evenly covering all particles, is interpreted as an ionomer layer, with a thickness of 1–2 nm, visible at the edges of the sample (Figure 7b). In contrast, at the EOL, there are regions where this ionomer layer is less than 0.5 nm. The lack of ionomer can affect the transportation of ions to the reaction sites, which would reduce the overall performance. Figure S3 shows additional TEM images across the cross-sectional view of the cathodic CL at the EOL.

Figure 7a and b and Figure S2 show representative images of the cross section at BOL. Similar behavior is seen throughout the whole cross section. In contrast, at the EOL (Figure S3) the degradation differs over the cross section of the catalyst layer, as seen when comparing images from the surface, middle, and bottom of the cathodic catalyst layer. While all regions show signs of degradation with particle sizes by increasing with similar growth rate from the observable view, the closer to the proton exchange membrane, the more closely packed the particles are to each other, with less empty carbon support areas, indicating that the catalyst particles tend to migrate toward the catalyst–membrane interface, in agreement with previous studies.<sup>45</sup> This points to the fact that while the IL-SEM measurement presented here gives insight in how the degradation progresses at the catalyst–GDL interface, it does not necessarily translate to how the degradation transpires throughout the whole catalyst layer.

Figure 8a presents the recorded cyclic voltammograms (CVs) that were recorded at the BOL and after each AST session. To ensure that the disassembling of the fuel cell and IL-SEM measurements did not affect the performance of the MEA, a similar electrochemical experiment was conducted without removing the MEA from the fuel cell nor performing IL-SEM between AST cycling protocols (Figure 8b). The CVs from both runs show similar behavior, with the absolute current decreasing significantly over time. The ECSA was calculated from the CVs by integrating the charge associated with the  $H_{\text{upd}}$  region up to an upper potential limit of 0.4  $V_{\text{RHE}}$ , showing initial ECSA values of 77.5 and 79.7  $\text{m}^2 \text{g}_{\text{Pt}}^{-1}$  for the MEA with and without IL-SEM between AST-sessions, respectively. After 100 AST cycles, a minor decrease in current in the  $H_{\text{upd}}$  region can be seen, whereas a significant loss in the  $H_{\text{upd}}$  features is observed with further cycling, which is reflected in the gradual loss of ECSA (Figure 8c and d). In absolute values, the two MEAs show a minor difference due to natural variances between the catalytic coated membranes. However, when expressing the change in ECSA as a percentage of initial surface area (Figure 8c), the ECSA losses of the two runs overlap, showing that the disassembling and the IL-SEM imaging between AST sessions do not affect the fuel cell performance. At the EOL, about 72% of the initial ECSA has been lost, which is similar to the change measured by other research groups using SW ASTs.<sup>44</sup> Besides the  $H_{\text{upd}}$  region, the Pt oxidation, reduction, and hydrogen desorption features have decreased as well, whereas the double layer stayed the same over the course of the degradation process.

To obtain information on how the change of Pt particles' size affects the fuel cell performance activity, polarization curves were performed under  $H_2$ /air at the anode/cathode at 80 °C and fully humidified gases (Figure 8e and f). The solid lines represent the polarization curves at different aging steps,





**Figure 7.** TEM images of the cathodic catalytic layer from BOL (a and b) and EOL (c and d). The ionomer layer, which can be seen around the Pt particles is thinner at EOL compared to BOL.

and the dashed lines show the HFR. In both fuel cell cases, the activity of the polarization curves (not *iR*-corrected) and the HFR are similar. The polarization curves of the fuel cell show a stable activity up to 4000 AST cycles, after which the activity starts to decrease slightly. Interestingly, the activity barely changes at the EOL even though the ECSA shows a more significant decline of around 72%. Harzer et al.<sup>44</sup> show a similar outcome in the decrease of the polarization curves after 10K SW AST cycles, whereas there is a more pronounced degradation of the activity after further AST cycling of 20K and 30K cycles. The discrepancy between lost ECSA without a coinciding loss of activity can be explained by the fact that as the particles grow, they favor a state that is more stable but also more catalytically active. The loss of ECSA as the particles grow is then compensated by the higher activity per surface area.<sup>67</sup> Moreover, an additional explanation is that the available Pt surface area at the EOL state is still sufficiently high to not significantly affect the reaction kinetics.

The IL-SEM and TEM images of the cathodic catalytic layer that were taken over the course of the aging protocol reveal several observations regarding degradation of the Pt nanoparticles. These observations are illustrated in Figure 9. Most particles observed by SEM grow, often without any nearby detectable particles to donate material, and in some cases, particles appear seemingly from nowhere. The explanation for this can be found in the TEM images. In the fresh CL, most particles are too small to be detected by SEM.

One of the observations is the shrinkage and disappearance of particles. Often these particles are close to other larger particles that have grown during the same period, which would indicate that these particles have shrunk, sometimes until not visible with SEM, due to Oswald ripening. However,

sometimes particles disappear completely, without any close neighbor to deposit material onto nor signs of shrinking earlier in the degradation process, which could be due to those particles having been detached completely from the carbon support and redeposited on a different location or removed with the exhaust.<sup>29</sup> Particles in the vicinity of each other tend to move toward one another and agglomerate, which can cause crystallite migration followed by coalescence to form larger particles, which often are elongated and nonspherical.

The PSD shows that larger particles (>5 nm) grow on average, meaning that the smaller particles (<5 nm) must be donating their material and shrinking on average. This is further supported by the TEM images, showing much fewer small particles (<5 nm) at the EOL than at the BOL, due to the instability of small nanoparticles.<sup>28,68,68</sup> Due to the average growth, less surface area is available for reactions per gram of Pt, which, at least in part, explains the loss in ECSA. Also, loss of ionomer means some particles have lower or no ionic contact with the support and cannot contribute to the effective ECSA.

From the IL-SEM images, some deformation of the carbon support can be observed, as well as some carbon that have vanished. However, the carbon support is still relatively stable compared to the nanoparticles in this type of AST, and the main observation regarding degradation seems to be growth and loss of Pt nanoparticles. The AST cycling protocol that was used used potentials within the range of standard fuel cell operation, and in that potential range carbon is mostly stable.<sup>42,69</sup>

In summary, the observations regarding degradation of the Pt nanoparticles are as follows:

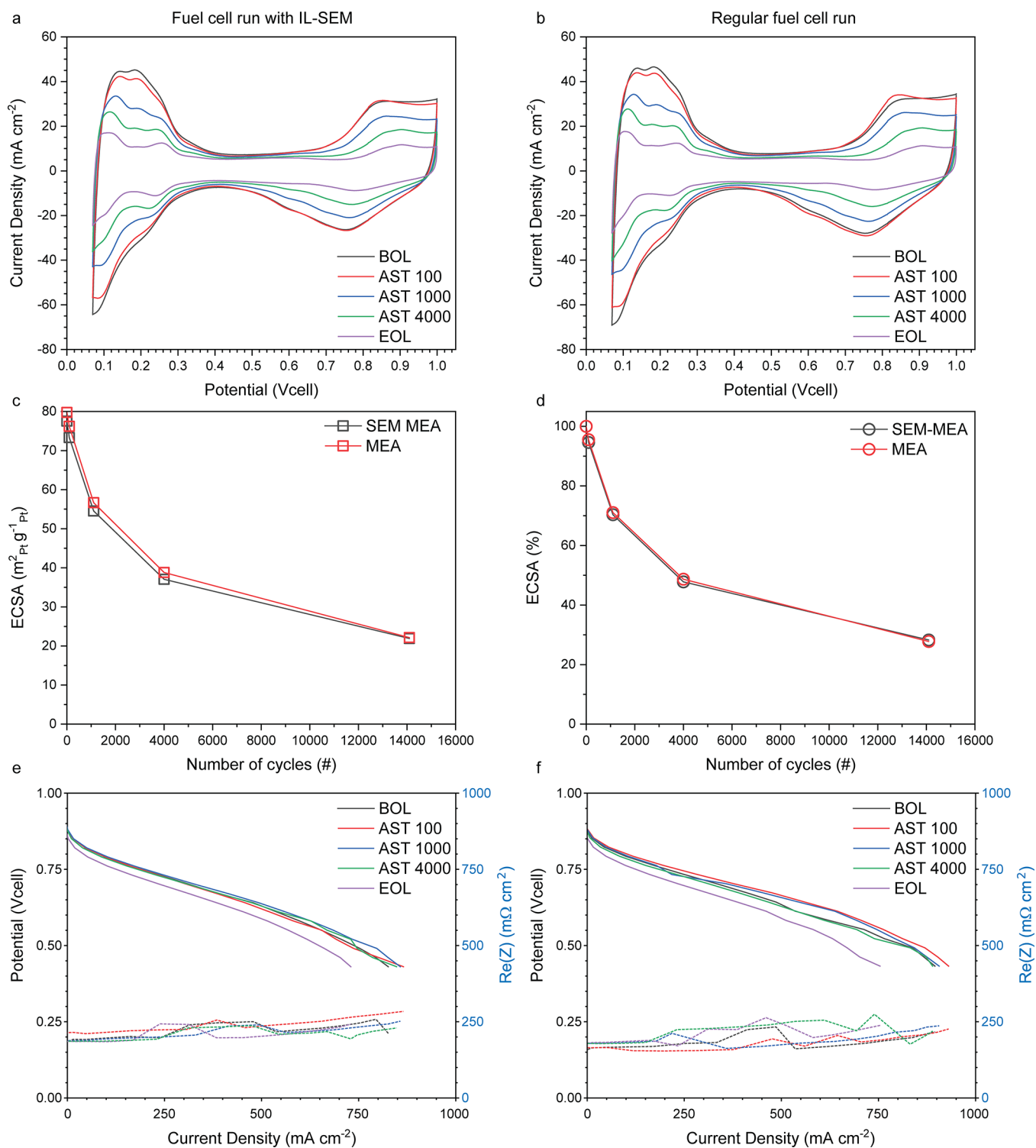


**Figure 8.** CVs after each AST session for an MEA (a) run with IL-SEM and (b) run without IL-SEM in the intermediary steps. The measured ECDSA values after each cycle for both samples are shown (c) as total surface area per gram Pt and (d) as a percentage of the initial ECDSA. Polarization curve (solid line) and HFR (dashed lines) of the MEA after each AST session run (e) with and (f) without IL-SEM.

1. Larger Pt particles tend to grow by absorbing dissolved material from smaller, less stable neighbor particles, via Oswald ripening (Figure 9 row 1).
2. A minor percentage of the larger particles shrink to the point of not being visible by SEM. Some particles disappear without showing signs of shrinking before,

indicating they have detached from the carbon support (Figure 9 row 2).

3. Particles grow until they merge with nearby neighbors (Figure 9 row 3).
4. Some particles grow during the initial ASTs, after which they start to shrink during the later AST sessions (Figure 9 row 4).

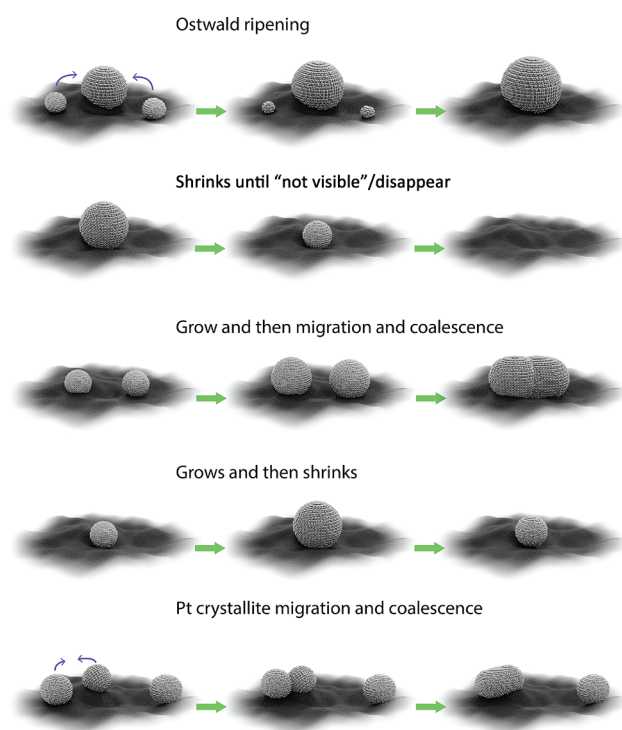


**Figure 9.** Schematic illustration of five different observations regarding degradation of the platinum nanoparticles that were observed in the IL-SEM.

5. Particles close to each other tend to merge via crystallite migration and coalescence, whereas particles further away do not move toward each other (Figure 9 row 5). Particles that grow by crystallite migration tend to form elongated particles.

## CONCLUSION

In this study, we investigate the degradation of the cathodic catalytic layer (CL) in a proton exchange membrane fuel cell (PEMFC) during optimal operation conditions in a potential range of 0.6 to 1.0  $V_{RHE}$ , to avoid strong degradation effects such as carbon corrosion that occurs above 1.0  $V_{RHE}$ , and under control to avoid fuel and air starvation. A square wave accelerated stress test (SW AST) was applied between 0.6 and 1.0  $V_{RHE}$ , corresponding to reduction and surface oxidation of Pt, respectively, to observe fundamental degradation of the cathodic CL. The degradation study was performed on a commercial membrane electrode assembly (MEA) with a Pt loading of 0.1/0.4  $mg_{Pt} cm^{-2}$  on the cathode/anode, respectively. The SW AST was conducted on the MEA with an increasing number of SW cycles each AST session, with  $H_2$ /argon on anode/cathode, at ambient pressure, 80 °C, and with 100% RH. Identical location scanning electrode microscopy (IL-SEM) images were taken at the beginning of life (BOL) and after each AST session until the end of life (EOL). Cross-sectional transmission electron microscopy (TEM) images of the cathodic CL were collected at BOL and EOL to observe the behavior of the electrocatalysts on the atomic scale. To verify that the IL-SEM sessions do not affect the degradation of the MEA, an identical experiment was run but without IL-SEM in-between AST session, and the electrochemical analysis of the electrochemical active surface area (ECSA) and polarization curves were compared between the two experiments.

Both MEAs showed similar electrochemical degradation after each AST session, with ECSA values being reduced by about 72% after 14,000 cycles. The decrease of the ECSA values per SW AST cycle was found to be similar to previously reported data.<sup>44</sup> The loss of ECSA corresponds to an average increase in particle size, as observed via IL-SEM and TEM imaging. At the BOL, the Pt nanoparticles are relatively similar in size and homogeneously spread over the carbon support. Over the course of the AST cycling, the Pt nanoparticles tend to grow either via Ostwald ripening or via crystallite migration and coalescence, depending on the local environment, creating larger more stable particles with lower surface area. Moreover, the TEM images show that the thickness of the ionomer layer has decreased, which could reduce the overall activity by reducing its ability to conduct protons. From this work, we suggest that IL-SEM techniques can be used in tandem with degradation techniques to gain more qualitative data on the degradation process of individual particles of the CL to gain insight in how to design better and more stable PEMFCs.

## ASSOCIATED CONTENT

### Supporting Information

The Supporting Information is available free of charge at <https://pubs.acs.org/doi/10.1021/acsaem.2c01790>.

TEM images of the cathodic CL and IL-SEM images from the beginning of life and after 100, 1000, 4000, and 14,000 cycles of the inlet, middle, and outlet regions (PDF)

## AUTHOR INFORMATION

### Corresponding Authors

**Victor Shokhen** – Department of Physics, Chalmers University of Technology, SE-412 96 Göteborg, Sweden; Competence Centre for Catalysis, Chalmers University of Technology, SE-412 96 Göteborg, Sweden; [orcid.org/0000-0002-9990-2041](https://orcid.org/0000-0002-9990-2041); Email: [shokhen@chalmers.se](mailto:shokhen@chalmers.se)

**Björn Wickman** – Department of Physics, Chalmers University of Technology, SE-412 96 Göteborg, Sweden; Competence Centre for Catalysis, Chalmers University of Technology, SE-412 96 Göteborg, Sweden; [orcid.org/0000-0001-7119-9529](https://orcid.org/0000-0001-7119-9529); Email: [bjorn.wickman@chalmers.se](mailto:bjorn.wickman@chalmers.se)

### Authors

**Linnéa Strandberg** – Department of Physics, Chalmers University of Technology, SE-412 96 Göteborg, Sweden; Competence Centre for Catalysis, Chalmers University of Technology, SE-412 96 Göteborg, Sweden

**Magnus Skoglundh** – Department of Chemistry and Chemical Engineering and Competence Centre for Catalysis, Chalmers University of Technology, SE-412 96 Göteborg, Sweden; [orcid.org/0000-0001-7946-7137](https://orcid.org/0000-0001-7946-7137)

Complete contact information is available at: <https://pubs.acs.org/doi/10.1021/acsaem.2c01790>

### Author Contributions

<sup>†</sup>V.S. and L.S. contributed equally to this paper

### Notes

The authors declare no competing financial interest.



## ACKNOWLEDGMENTS

This project is financially supported by the Swedish Foundation for Strategic Research (Project No. ARC19-0026) and the Swedish Research Council (Project No. 2018-03927), and it is performed within the Competence Centre for Catalysis, which is hosted by Chalmers University of Technology and financially supported by the Swedish Energy Agency (Project No. 52689-1) and the member companies ECAPS, Johnson Matthey, Perstorp, Powercell, Preem, Scania CV, Umicore, and Volvo Group. Physical characterization was performed at Chalmers Materials Analysis Laboratory (CMAL).

## REFERENCES

- (1) Staffell, I.; Scamman, D.; Velazquez Abad, A.; Balcombe, P.; Dodds, P. E.; Ekins, P.; Shah, N.; Ward, K. R. The role of hydrogen and fuel cells in the global energy system. *Energy Environ. Sci.* **2019**, *12*, 463–491.
- (2) Probst, B.; Touboul, S.; Glachant, M.; Dechezelepretre, A. Global trends in the invention and diffusion of climate change mitigation technologies. *Nature Energy* **2021**, *6*, 1077–1086.
- (3) Stamenkovic, V. R.; Strmcnik, D.; Lopes, P. P.; Markovic, N. M. Energy and fuels from electrochemical interfaces. *Nature materials* **2017**, *16*, 57–69.
- (4) Debe, M. K. Electrocatalyst approaches and challenges for automotive fuel cells. *Nature* **2012**, *486*, 43–51.
- (5) Cano, Z. P.; Banham, D.; Ye, S.; Hintennach, A.; Lu, J.; Fowler, M.; Chen, Z. Batteries and fuel cells for emerging electric vehicle markets. *Nature Energy* **2018**, *3*, 279–289.
- (6) Eberle, U.; Müller, B.; Von Helmolt, R. Fuel cell electric vehicles and hydrogen infrastructure: status 2012. *Energy Environ. Sci.* **2012**, *5*, 8780–8798.
- (7) Cullen, D. A.; Neyerlin, K. C.; Ahluwalia, R. K.; Mukundan, R.; More, K. L.; Borup, R. L.; Weber, A. Z.; Myers, D. J.; Kusoglu, A. New roads and challenges for fuel cells in heavy-duty transportation. *Nature energy* **2021**, *6*, 462–474.
- (8) Yoshida, T.; Kojima, K. Toyota MIRAI fuel cell vehicle and progress toward a future hydrogen society. *Electrochemical Society Interface* **2015**, *24*, 45.
- (9) Marić, R.; Gebauer, C.; Nesselberger, M.; Hasché, F.; Strasser, P. Towards a Harmonized Accelerated Stress Test Protocol for Fuel Starvation Induced Cell Reversal Events in PEM Fuel Cells: The Effect of Pulse Duration. *J. Electrochem. Soc.* **2020**, *167*, 124520.
- (10) Mittermeier, T.; Weiß, A.; Hasché, F.; Hübner, G.; Gasteiger, H. A. PEM fuel cell start-up/shut-down losses vs temperature for non-graphitized and graphitized cathode carbon supports. *J. Electrochem. Soc.* **2017**, *164*, F127.
- (11) Durst, J.; Lamibrac, A.; Charlot, F.; Dillet, J.; Castanheira, L. F.; Maranzana, G.; Dubau, L.; Maillard, F.; Chatenet, M.; Lottin, O. Degradation heterogeneities induced by repetitive start/stop events in proton exchange membrane fuel cell: Inlet vs. outlet and channel vs. land. *Applied Catalysis B: Environmental* **2013**, *138*, 416–426.
- (12) Stariha, S.; Macauley, N.; Sneed, B. T.; Langlois, D.; More, K. L.; Mukundan, R.; Borup, R. L. Recent advances in catalyst accelerated stress tests for polymer electrolyte membrane fuel cells. *J. Electrochem. Soc.* **2018**, *165*, F492.
- (13) Takei, C.; Kakinuma, K.; Kawashima, K.; Tashiro, K.; Watanabe, M.; Uchida, M. Load cycle durability of a graphitized carbon black-supported platinum catalyst in polymer electrolyte fuel cell cathodes. *J. Power Sources* **2016**, *324*, 729–737.
- (14) Yoda, T.; Uchida, H.; Watanabe, M. Effects of operating potential and temperature on degradation of electrocatalyst layer for PEFCs. *Electrochimica acta* **2007**, *52*, 5997–6005.
- (15) Mittermeier, T.; Weiß, A.; Hasché, F.; Gasteiger, H. A. PEM fuel cell start-up/shut-down losses vs relative humidity: the impact of water in the electrode layer on carbon corrosion. *J. Electrochem. Soc.* **2018**, *165*, F1349.
- (16) Petrone, R.; Hissel, D.; Péra, M.; Chamagne, D.; Gouriveau, R. Accelerated stress test procedures for PEM fuel cells under actual load constraints: State-of-art and proposals. *Int. J. Hydrogen Energy* **2015**, *40*, 12489–12505.
- (17) Jiao, K.; Xuan, J.; Du, Q.; Bao, Z.; Xie, B.; Wang, B.; Zhao, Y.; Fan, L.; Wang, H.; Hou, Z.; Huo, S.; Brandon, P. N.; Yin, Y.; Guiver, M. D. Designing the next generation of proton-exchange membrane fuel cells. *Nature* **2021**, *595*, 361–369.
- (18) Chung, D. Y.; Yoo, J. M.; Sung, Y.-E. Highly durable and active Pt-based nanoscale design for fuel-cell oxygen-reduction electrocatalysts. *Advanced materials* **2018**, *30*, 1704123.
- (19) Xiao, F.; Wang, Y.-C.; Wu, Z.-P.; Chen, G.; Yang, F.; Zhu, S.; Siddharth, K.; Kong, Z.; Lu, A.; Li, J.-C.; Zhong, C.-J.; Zhou, Z.-Y.; Shao, M. Recent advances in electrocatalysts for proton exchange membrane fuel cells and alkaline membrane fuel cells. *Adv. Mater.* **2021**, *33*, 2006292.
- (20) Fuchs, T.; Drnec, J.; Calle-Vallejo, F.; Stubbs, N.; Sandbeck, D. J.; Ruge, M.; Cherevko, S.; Harrington, D. A.; Magnussen, O. M. Structure dependency of the atomic-scale mechanisms of platinum electro-oxidation and dissolution. *Nature Catalysis* **2020**, *3*, 754–761.
- (21) Topalov, A. A.; Katsounaros, I.; Auinger, M.; Cherevko, S.; Meier, J. C.; Klemm, S. O.; Mayrhofer, K. J. Dissolution of platinum: limits for the deployment of electrochemical energy conversion? *Angew. Chem., Int. Ed.* **2012**, *51*, 12613–12615.
- (22) Kodama, K.; Nagai, T.; Kuwaki, A.; Jinnouchi, R.; Morimoto, Y. Challenges in applying highly active Pt-based nanostructured catalysts for oxygen reduction reactions to fuel cell vehicles. *Nat. Nanotechnol.* **2021**, *16*, 140–147.
- (23) Simonsen, S. B.; Chorkendorff, I.; Dahl, S.; Skoglundh, M.; Sehested, J.; Helveg, S. Direct observations of oxygen-induced platinum nanoparticle ripening studied by in situ TEM. *J. Am. Chem. Soc.* **2010**, *132*, 7968–7975.
- (24) Simonsen, S. B.; Chorkendorff, I.; Dahl, S.; Skoglundh, M.; Sehested, J.; Helveg, S. Ostwald ripening in a Pt/SiO<sub>2</sub> model catalyst studied by in situ TEM. *Journal of catalysis* **2011**, *281*, 147–155.
- (25) Simonsen, S. B.; Chorkendorff, I.; Dahl, S.; Skoglundh, M.; Helveg, S. Coarsening of Pd nanoparticles in an oxidizing atmosphere studied by in situ TEM. *Surf. Sci.* **2016**, *648*, 278–283.
- (26) Zhang, H.; Shen, P. K. Recent development of polymer electrolyte membranes for fuel cells. *Chem. Rev.* **2012**, *112*, 2780–2832.
- (27) Kusoglu, A.; Weber, A. Z. New insights into perfluorinated sulfonic-acid ionomers. *Chem. Rev.* **2017**, *117*, 987–1104.
- (28) Cherevko, S.; Kulyk, N.; Mayrhofer, K. J. Durability of platinum-based fuel cell electrocatalysts: Dissolution of bulk and nanoscale platinum. *Nano energy* **2016**, *29*, 275–298.
- (29) Dubau, L.; Castanheira, L.; Maillard, F.; Chatenet, M.; Lottin, O.; Maranzana, G.; Dillet, J.; Lamibrac, A.; Perrin, J.-C.; Moukheiber, E.; ElKaddouri, A.; De Moor, G.; Flandin, L.; Caqué, N. A review of PEM fuel cell durability: materials degradation, local heterogeneities of aging and possible mitigation strategies. *Wiley Interdisciplinary Reviews: Energy and Environment* **2014**, *3*, 540–560.
- (30) Kodama, K.; Motobayashi, K.; Shinohara, A.; Hasegawa, N.; Kudo, K.; Jinnouchi, R.; Osawa, M.; Morimoto, Y. Effect of the side-chain structure of perfluoro-sulfonic acid ionomers on the oxygen reduction reaction on the surface of Pt. *ACS Catal.* **2018**, *8*, 694–700.
- (31) Takeshita, T.; Kamitaka, Y.; Shinozaki, K.; Kodama, K.; Morimoto, Y. Evaluation of ionomer coverage on Pt catalysts in polymer electrolyte membrane fuel cells by CO stripping voltammetry and its effect on oxygen reduction reaction activity. *J. Electroanal. Chem.* **2020**, *871*, 114250.
- (32) Jinnouchi, R.; Kudo, K.; Kodama, K.; Kitano, N.; Suzuki, T.; Minami, S.; Shinozaki, K.; Hasegawa, N.; Shinohara, A. The role of oxygen-permeable ionomer for polymer electrolyte fuel cells. *Nat. Commun.* **2021**, *12*, 4952.
- (33) Xu, K.; Zhao, X.; Hu, X.; Guo, Z.; Ye, Q.; Li, L.; Song, J.; Song, P. The review of the degradation mechanism of the catalyst layer of membrane electrode assembly in the proton exchange membrane fuel



cell. *IOP Conference Series: Earth and Environmental Science* **2020**, 558, 052041.

(34) Young, A.; Stumper, J.; Knights, S.; Gyenge, E. Ionomer degradation in polymer electrolyte membrane fuel cells. *J. Electrochem. Soc.* **2010**, 157, B425.

(35) Zatoň, M.; Rozière, J.; Jones, D. Current understanding of chemical degradation mechanisms of perfluorosulfonic acid membranes and their mitigation strategies: a review. *Sustainable Energy & Fuels* **2017**, 1, 409–438.

(36) Young, A.; Stumper, J.; Gyenge, E. Characterizing the structural degradation in a PEMFC cathode catalyst layer: carbon corrosion. *J. Electrochem. Soc.* **2009**, 156, B913.

(37) Wang, C.; Ricketts, M.; Soleymani, A. P.; Jankovic, J.; Waldecker, J.; Chen, J. Effect of Carbon Support Characteristics on Fuel Cell Durability in Accelerated Stress Testing. *J. Electrochem. Soc.* **2021**, 168, 044507.

(38) Maass, S.; Finsterwalder, F.; Frank, G.; Hartmann, R.; Merten, C. Carbon support oxidation in PEM fuel cell cathodes. *J. Power Sources* **2008**, 176, 444–451.

(39) Pizzutilo, E.; Geiger, S.; Grote, J.-P.; Mingers, A.; Mayrhofer, K. J. J.; Arenz, M.; Cherevko, S. On the need of improved accelerated degradation protocols (ADPs): examination of platinum dissolution and carbon corrosion in half-cell tests. *J. Electrochem. Soc.* **2016**, 163, F1510.

(40) Yu, Y.; Li, H.; Wang, H.; Yuan, X.-Z.; Wang, G.; Pan, M. A review on performance degradation of proton exchange membrane fuel cells during startup and shutdown processes: Causes, consequences, and mitigation strategies. *J. Power Sources* **2012**, 205, 10–23.

(41) Reiser, C. A.; Bregoli, L.; Patterson, T. W.; Yi, J. S.; Yang, J. D.; Perry, M. L.; Jarvi, T. D. A reverse-current decay mechanism for fuel cells. *Electrochem. Solid-State Lett.* **2005**, 8, A273.

(42) Borup, R. L.; Papadias, D. D.; Mukundan, R.; Spornjak, D.; Langlois, D. A.; Ahluwalia, R.; More, K. L.; Grot, S. Carbon corrosion in PEM fuel cells during drive cycle operation. *Ecs Transactions* **2015**, 69, 1029.

(43) Kangasniemi, K. H.; Condit, D.; Jarvi, T. Characterization of vulcan electrochemically oxidized under simulated PEM fuel cell conditions. *J. Electrochem. Soc.* **2004**, 151, No. E125.

(44) Harzer, G. S.; Schwämmlein, J. N.; Damjanović, A. M.; Ghosh, S.; Gasteiger, H. A. Cathode loading impact on voltage cycling induced PEMFC degradation: a voltage loss analysis. *J. Electrochem. Soc.* **2018**, 165, F3118.

(45) Ferreira, P. J.; Shao-Horn, Y.; Morgan, D.; Makharia, R.; Kocha, S.; Gasteiger, H. A. Instability of Pt/C electrocatalysts in proton exchange membrane fuel cells: a mechanistic investigation. *J. Electrochem. Soc.* **2005**, 152, A2256.

(46) Ren, X.; Wang, Y.; Liu, A.; Zhang, Z.; Lv, Q.; Liu, B. Current progress and performance improvement of Pt/C catalysts for fuel cells. *Journal of Materials Chemistry A* **2020**, 8, 24284–24306.

(47) Wang, X. X.; Swihart, M. T.; Wu, G. Achievements, challenges and perspectives on cathode catalysts in proton exchange membrane fuel cells for transportation. *Nature Catalysis* **2019**, 2, 578–589.

(48) Orfanidi, A.; Madkikar, P.; El-Sayed, H. A.; Harzer, G. S.; Kratky, T.; Gasteiger, H. The key to high performance low Pt loaded electrodes. *J. Electrochem. Soc.* **2017**, 164, F418.

(49) Kongkanand, A.; Mathias, M. F. The priority and challenge of high-power performance of low-platinum proton-exchange membrane fuel cells. *Journal of physical chemistry letters* **2016**, 7, 1127–1137.

(50) Gilbert, J. A.; Kariuki, N. N.; Subbaraman, R.; Kropf, A. J.; Smith, M. C.; Holby, E. F.; Morgan, D.; Myers, D. J. In situ anomalous small-angle X-ray scattering studies of platinum nanoparticle fuel cell electrocatalyst degradation. *J. Am. Chem. Soc.* **2012**, 134, 14823–14833.

(51) Hodnik, N.; Cherevko, S. Spot the difference at the nanoscale: identical location electron microscopy in electrocatalysis. *Current opinion in electrochemistry* **2019**, 15, 73–82.

(52) Zadick, A.; Dubau, L.; Demirci, U. B.; Chatenet, M. Effects of Pd nanoparticle size and solution reducer strength on Pd/C

electrocatalyst stability in alkaline electrolyte. *J. Electrochem. Soc.* **2016**, 163, F781.

(53) Lafforgue, C.; Maillard, F.; Martin, V.; Dubau, L.; Chatenet, M. Degradation of carbon-supported platinum-group-metal electrocatalysts in alkaline media studied by in situ Fourier transform infrared spectroscopy and identical-location transmission electron microscopy. *ACS Catal.* **2019**, 9, 5613–5622.

(54) Yu, H.; Zachman, M. J.; Li, C.; Hu, L.; Kariuki, N. N.; Mukundan, R.; Xie, J.; Neyerlin, K. C.; Myers, D. J.; Cullen, D. A. Recreating Fuel Cell Catalyst Degradation in Aqueous Environments for Identical-Location Scanning Transmission Electron Microscopy Studies. *ACS Appl. Mater. Interfaces* **2022**, 14, 20418–20429.

(55) Hodnik, N.; Zorko, M.; Jozinović, B.; Bele, M.; Dražič, G.; Hočvar, S.; Gaberšček, M. Severe accelerated degradation of PEMFC platinum catalyst: A thin film IL-SEM study. *Electrochem. Commun.* **2013**, 30, 75–78.

(56) Zorko, M.; Jozinović, B.; Bele, M.; Hodnik, N.; Gaberšček, M. SEM method for direct visual tracking of nanoscale morphological changes of platinum based electrocatalysts on fixed locations upon electrochemical or thermal treatments. *Ultramicroscopy* **2014**, 140, 44–50.

(57) Hodnik, N.; Zorko, M.; Bele, M.; Hočvar, S.; Gaberšček, M. Identical location scanning electron microscopy: a case study of electrochemical degradation of PtNi nanoparticles using a new nondestructive method. *J. Phys. Chem. C* **2012**, 116, 21326–21333.

(58) Fan, J.; Chen, M.; Zhao, Z.; Zhang, Z.; Ye, S.; Xu, S.; Wang, H.; Li, H. Bridging the gap between highly active oxygen reduction reaction catalysts and effective catalyst layers for proton exchange membrane fuel cells. *Nature Energy* **2021**, 6, 475–486.

(59) Lafforgue, C.; Chatenet, M.; Dubau, L.; Dekel, D. R. Accelerated Stress Test of Pt/C Nanoparticles in an Interface with an Anion-Exchange Membrane- An Identical-Location Transmission Electron Microscopy Study. *ACS Catal.* **2018**, 8, 1278–1286.

(60) Alinejad, S.; Inaba, M.; Schröder, J.; Du, J.; Quinson, J.; Zana, A.; Arenz, M. Testing fuel cell catalysts under more realistic reaction conditions: accelerated stress tests in a gas diffusion electrode setup. *Journal of Physics: Energy* **2020**, 2, 024003.

(61) Martens, I.; Vamvakeros, A.; Chattot, R.; Blanco, M. V.; Rasola, M.; Pusa, J.; Jacques, S. D.; Bizzotto, D.; Wilkinson, D. P.; Ruffmann, B.; Heidemann, S.; Honkimäki, V.; Drnec, J. X-ray transparent proton-exchange membrane fuel cell design for in situ wide and small angle scattering tomography. *J. Power Sources* **2019**, 437, 226906.

(62) Petkov, V.; Maswadeh, Y.; Zhao, Y.; Lu, A.; Cronk, H.; Chang, F.; Shan, S.; Kareem, H.; Luo, J.; Zhong, C.-J.; Shastri, S.; Kenesei, P. Nanoalloy catalysts inside fuel cells: An atomic-level perspective on the functionality by combined in operando x-ray spectroscopy and total scattering. *Nano Energy* **2018**, 49, 209–220.

(63) Uchimura, M.; Kocha, S. S. The impact of cycle profile on PEMFC durability. *Ecs Transactions* **2007**, 11, 1215.

(64) Brummer, S. The use of large anodic galvanostatic transients to evaluate the maximum adsorption on platinum from formic acid solutions. *J. Phys. Chem.* **1965**, 69, 562–571.

(65) Wang, Y.; Wang, L.; Ji, X.; Zhou, Y.; Wu, M. Experimental and Numerical Study of Proton Exchange Membrane Fuel Cells with a Novel Compound Flow Field. *ACS omega* **2021**, 6, 21892–21899.

(66) Martens, I.; Vamvakeros, A.; Martinez, N.; Chattot, R.; Pusa, J.; Blanco, M. V.; Fisher, E. A.; Asset, T.; Escibano, S.; Micoud, F.; Starr, T.; Coelho, A.; Honkimäki, V.; Bizzotto, D.; Wilkinson, D. P.; Jacques, S. D. M.; Maillard, F.; Dubau, L.; Lyonnard, S.; Morin, A.; Drnec, J. Imaging heterogeneous electrocatalyst stability and decoupling degradation mechanisms in operating hydrogen fuel cells. *ACS Energy Letters* **2021**, 6, 2742–2749.

(67) Perez-Alonso, F. J.; McCarthy, D. N.; Nierhoff, A.; Hernandez-Fernandez, P.; Strebel, C.; Stephens, I. E.; Nielsen, J. H.; Chorkendorff, I. The effect of size on the oxygen electroreduction activity of mass-selected platinum nanoparticles. *Angew. Chem., Int. Ed.* **2012**, 51, 4641–4643.

- (68) Hiraoka, F.; Matsuzawa, K.; Mitsushima, S. Degradation of Pt/C under various potential cycling patterns. *Electrocatalysis* **2013**, *4*, 10–16.
- (69) Meyers, J. P.; Darling, R. M. Model of Carbon Corrosion in PEM Fuel Cells. *J. Electrochem. Soc.* **2006**, *153*, A1432.

## Recommended by ACS

### Recreating Fuel Cell Catalyst Degradation in Aqueous Environments for Identical-Location Scanning Transmission Electron Microscopy Studies

Haoran Yu, David A. Cullen, *et al.*

MARCH 01, 2022

ACS APPLIED MATERIALS & INTERFACES

READ 

### Visualization of Hydrogen Evolution at Individual Platinum Nanoparticles at a Buried Interface

Rui Gao, Henry S. White, *et al.*

APRIL 22, 2020

JOURNAL OF THE AMERICAN CHEMICAL SOCIETY

READ 

### Effect of Pt and Ionomer Distribution on Polymer Electrolyte Fuel Cell Performance and Durability

Aki Kobayashi, Makoto Uchida, *et al.*

FEBRUARY 04, 2021

ACS APPLIED ENERGY MATERIALS

READ 

### Enhancement of the Catalytic Activity and Load Cycle Durability of a PtCo Alloy Cathode Catalyst Supported on Ta-Doped SnO<sub>2</sub> with a Unique Fused Aggregated Netwo...

Katsuyoshi Kakinuma, Makoto Uchida, *et al.*

JUNE 15, 2020

ACS APPLIED ENERGY MATERIALS

READ 

Get More Suggestions >